

Negative Fermi-level Pinning Effect of Metal/n-GaAs(001) Junction with Graphene Interlayer

Hoon Hahn Yoon,¹ Wonho Song,¹ Sungchul Jung,¹ Junhyung Kim,² Kyuhyung Mo,¹ Gahyun Choi,¹ Hu Young Jeong,³ Jong Hoon Lee,³ and Kibog Park^{1,2,*}

¹*Department of Physics, Ulsan National Institute of Science and Technology (UNIST), Ulsan 44919, Republic of Korea*

²*School of Electrical and Computer Engineering,*

Ulsan National Institute of Science and Technology (UNIST), Ulsan 44919, Republic of Korea

³*UNIST Central Research Facilities (UCRF), Ulsan National Institute of Science and Technology (UNIST), Ulsan 44919, Republic of Korea*

It is demonstrated that the electric dipole layer due to the overlapping of electron wavefunctions at metal/graphene contact results in negative Fermi-level pinning effect on the region of GaAs surface with low interface-trap density in metal/graphene/n-GaAs(001) junction. The graphene interlayer takes a role of diffusion barrier preventing the atomic intermixing at interface and preserving the low interface-trap density region. The negative Fermi-level pinning effect is supported by the Schottky barrier decreasing as metal work-function increasing. Our work shows that the graphene interlayer can invert the effective work-function of metal between *high* and *low*, making it possible to form both Schottky and Ohmic-like contacts with identical (particularly *high* work-function) metal electrodes on a semiconductor substrate possessing low surface-state density.

I. INTRODUCTION

The interfacial physics and chemistry are key elements in understanding the electrostatic environment and the associated carrier transport at metal/graphene interface. The change of electrostatic potential across metal/graphene interface is determined by not only the electron transfer between metal and graphene caused by the difference in work-function but also the formation of an electric dipole layer originating from the off-centric distribution of interacting electrons at the interface [1–3]. The electrical properties of metal/graphene and graphene/semiconductor contacts have been studied actively as separate physical systems [4, 5]. However, the charge carrier transport across metal/graphene/semiconductor junction as a whole, particularly taking into account the interaction dipole charges at metal/graphene contact, has not received proper attention. The interests in metal/graphene/semiconductor junction stem mainly from the possibility of modulating the electron energy barrier at interface with the graphene interlayer [6–10]. Recently, it has been reported that the atomically-impermeable and electronically-transparent properties of graphene inserted at metal/n-Si(001) junctions can be used to form an intact Schottky contact and investigate the interface Fermi-level pinning effect [6]. The graphene interlayer prevents the interface intermixing of metal and semiconductor atoms which occurs on the region of Si surface with very thin or no native oxide layers and leads to the formation of small-area patches with low local Schottky barriers. In this study, the graphene layer inserted at metal/n-GaAs(001) junction is found to bring about a different phenomenon although it still plays a role of diffusion barrier. It is known that the reconstructed surface of III-V compound semiconductor contains gen-

erally a low density of surface states within its band gap unless the surface structure gets compromised by some extrinsic factors including defects, oxidation, and atomic intermixing with other materials [11]. Accordingly, the regions on the surface of our GaAs(001) substrate with very thin or no native oxide layer is considered also to possess a relatively low density of surface states. However, the material intermixing on those low-surface-state regions, occurring during metal deposition, can induce a substantial amount of interface-trap states similarly to the region of GaAs surface with normal native oxides. Then, the entire region of metal/n-GaAs(001) junction will be under relatively strong interface Fermi-level pinning effect. On the other hand, if a graphene layer is inserted at metal/n-GaAs(001) interface, the material intermixing on the regions with very thin or no native oxide layer no longer occurs and thus those regions can stay with a small density of interface-trap states, bearing pretty weak Fermi-level pinning [12–17]. From the growth mechanism of native oxide, the regions with low interface-trap density will be small in size and randomly scattered on the GaAs surface. Due to the strong Fermi-level pinning on the prevailing surrounding area, the metal-dependent variation of current-voltage (I-V) characteristics of metal/graphene/GaAs junction is expected to originate from the small patches of low interface-trap density [18, 19].

II. EXPERIMENTAL SECTION

A. Device Fabrication

The metal/GaAs and metal/graphene/GaAs junctions were prepared as follows. The Si-doped n-type ($N_D \simeq 5 \times 10^{16} \text{ cm}^{-3}$) GaAs wafer grown by the vertical gradi-

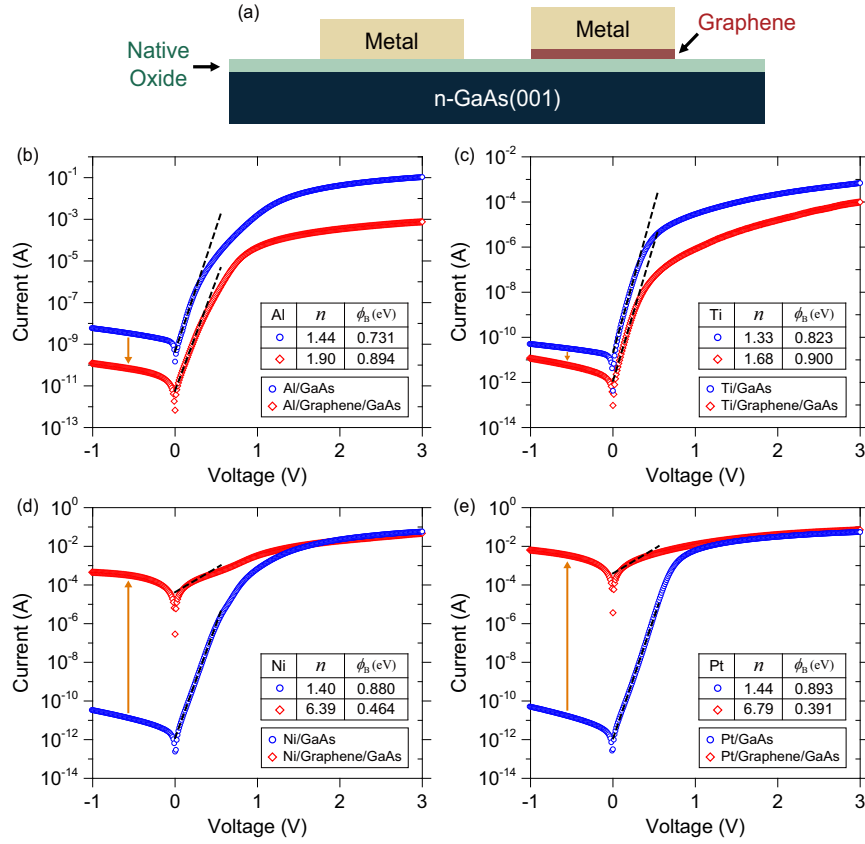


FIG. 1. Device schematic and I-V measurements. (a) Schematic of metal/GaAs with and without a graphene interlayer. (b)-(e) I-V curves measured on the metal/GaAs and metal/graphene/GaAs junctions with Al (b), Ti (c), Ni (d), and Pt (e) electrodes. Averaged over several different junctions, the Schottky barrier ϕ_B and ideality factor n for each metal are listed in the table inset.

ent freeze (VGF) method was purchased from the MTI Corporation. The GaAs substrate was first etched in a 1:1 $\text{NH}_4\text{OH}:\text{H}_2\text{O}$ solution for 1 min followed by DI water rinsing [20]. After that, Ti/Pt/Au (50/200/5000 Å) ohmic contacts were formed near the edge of GaAs substrate by using e-beam evaporation and rapid thermal annealing at 400 °C for 300 sec [21]. The sample was treated in a 1:1 $\text{NH}_4\text{OH}:\text{H}_2\text{O}$ etching solution for 3 min followed by DI water rinsing again right before the graphene transfer. The monolayer graphene synthesized on a Cu foil with chemical vapor deposition (CVD) was purchased from the Graphene Supermarket. In order to minimize the trapping of water molecules between graphene and GaAs surface and the residues during the transfer process [22], we used the dry transfer method adopting thermal release tapes. The graphene layer was partially transferred on the GaAs surface in order to form metal/GaAs and metal/graphene/GaAs junctions simultaneously on the same GaAs substrate. The structural qualities of transferred graphene were examined with Raman spectrum measurements (see Supporting Information for the Raman spectrum measurements) [23]. After the graphene transfer, circular metal electrodes (Al,

Ti, Ni, and Pt) of average diameter $\sim 500 \mu\text{m}$ were deposited through a shadow mask on the sample surface by using e-beam evaporation. The metal/GaAs junctions were formed on the graphene-uncovered area. Finally, the graphene uncovered by metal electrodes was removed with reactive ion etching (RIE) to isolate each junction.

B. Current-Voltage Measurement

The schematic of metal/GaAs junctions with and without a graphene interlayer is illustrated in Figure 1a. Figure 1b-e show the I-V characteristics of metal/GaAs and metal/graphene/GaAs junctions. As shown in Figure 1b,c, the Al/graphene/GaAs and Ti/graphene/GaAs junctions possess the typical rectifying characteristics. In fact, their reverse bias currents are somewhat smaller (more rectifying) than the Al/GaAs and Ti/GaAs junctions. On the other hand, the reverse bias currents of Ni/graphene/GaAs and Pt/graphene/GaAs junctions are significantly larger than those of Ni/GaAs and Pt/GaAs junctions (Figure 1d,e). The rectifying behaviors of both junc-

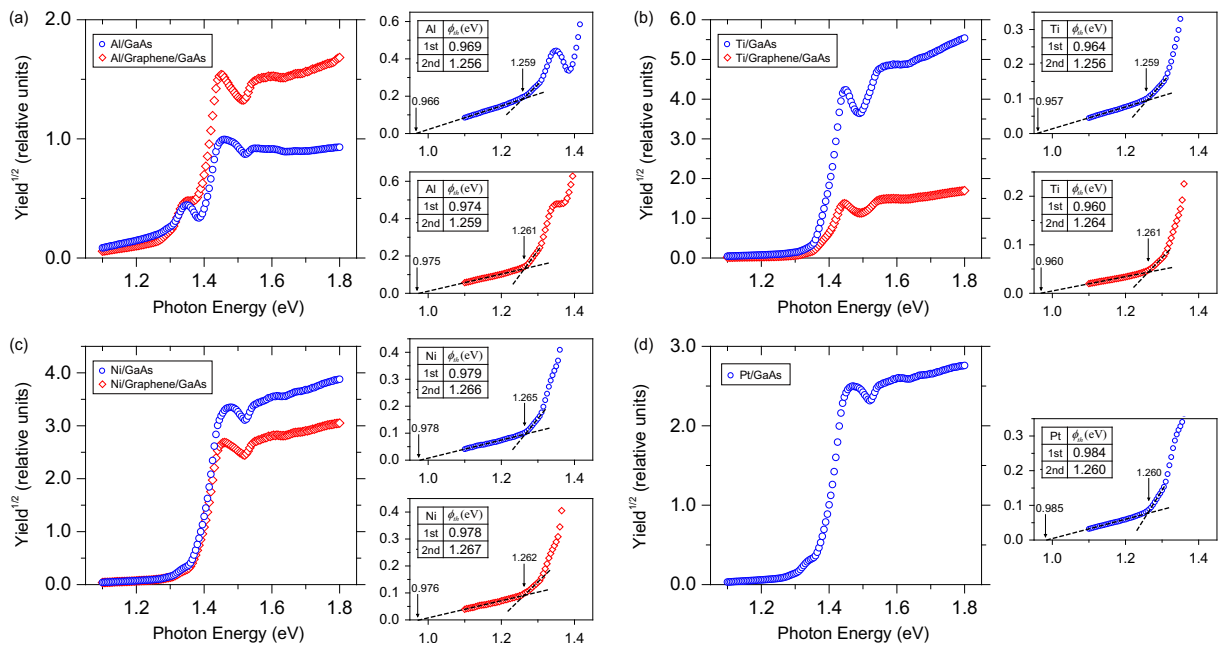


FIG. 2. IPE measurements. (a)-(d) Square root of IPE quantum yield as a function of photon energy measured on the metal/GaAs and metal/graphene/GaAs junctions with Al (a), Ti (b), Ni (c), and Pt (d) electrodes. The magnified views of the threshold region with linear extrapolation are also shown. Averaged over several different junctions, two IPE thresholds ϕ_{th} are listed in the table inset of magnified view.

tions have almost disappeared, turning into Ohmic-like ones. This is quite counter-intuitive since the local Schottky barrier formed on the region of GaAs surface with low interface-trap density is expected to be low for Al/graphene/GaAs and Ti/graphene/GaAs junctions and high for Ni/graphene/GaAs and Pt/graphene/GaAs junctions when considering the difference in metal work-function.

C. Internal Photoemission Measurement

The Internal Photoemission (IPE) yield spectra [6, 24, 25] for metal/GaAs and metal/graphene/GaAs junctions are shown in Figure 2. Since the IPE measurement reveals the motion of ballistic electron across the junction interface, its signals will be contributed collectively by all regions in the junction. However, if a junction is mostly uniform and only a small areal fraction of isolated patches exists with their interface energy barriers different from those on the uniform surrounding region, the IPE spectrum will be dominated by the prevailing region and the contribution from the small patches will be almost invisible. In the IPE spectra of metal/GaAs junctions, two thresholds ϕ_{th} for the conduction band minima (Γ and L valleys) of GaAs [26] are clearly observed. The first threshold represents the commonly accepted Schottky barrier of metal/GaAs junction, which reflects the electron transmission from metal into the Γ valley in GaAs. The additional transmission into the L valley

in GaAs corresponds to the second threshold. The gap between first and second thresholds is about ~ 0.29 eV, which is in excellent agreement with the known energy separation between Γ and L valleys. However, the observation of additional transmission into the X valley of GaAs is disturbed by the humps of IPE yield around 1.33 eV [27] (see Supporting Information for details on the direct optical excitation from localized interface states). Since the two thresholds are extracted to be pretty much identical for all four metal electrodes (Al, Ti, Ni, Pt) and no signature for additional threshold is observed, the Fermi-level pinning can be concluded to be strong uniformly throughout the entire metal/GaAs junction as known well. The metal/graphene/GaAs junctions also show two common thresholds in their IPE spectra for Al, Ti, and Ni electrodes which are quite similar to those for the metal/GaAs junctions. In case of Pt/graphene/GaAs junction, the large leakage current, confirmed in the I-V curve (Figure 1e), overwhelmed the photocurrent completely so that we could not determine the corresponding IPE yield at all (Figure 2d). The similarity in the IPE thresholds of metal/graphene/GaAs junction for different metal electrodes implies that the Fermi-level pinning is strong in the vast majority of junction area where the regular oxide layer is expected to reside and bear high interface-trap density. Here, there are several things to note about characterizing the fabricated junctions. All transport measurements including I-V and IPE measurements were carried out at room temperature. The power of incident light was measured separately by using a pho-

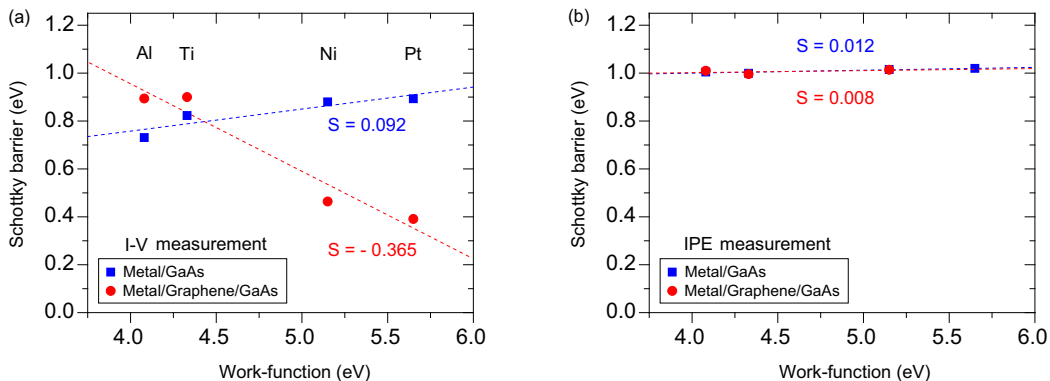


FIG. 3. Measured pinning strength. I-V extracted (a) and IPE extracted (b) Schottky barriers of metal/GaAs and metal/graphene/GaAs junctions as a function of metal work-function. The extracted pinning factor $S = \partial\phi_B/\partial\phi_M$ is labeled for each case.

todiode, HAMAMATSU S2281-04 (Si photodiode for the wavelength of 200-1180 nm) for acquiring the quantum yield of IPE[6, 24, 25]. After the measurements of electrical properties, the layer structures of fabricated junctions were examined by taking transmission electron microscope (TEM) images (see Supporting Information for the TEM images) [28–30].

III. RESULTS AND DISCUSSION

A. Negative Fermi-level Pinning Effect

Averaged over several different junctions, the Schottky barriers of metal/GaAs and metal/graphene/GaAs junctions were obtained from the I-V and IPE measurements. They were determined by either fitting the measured I-V curves shown in Figure 1 to the thermionic-emission theory [31] or extracting the first threshold of IPE yield shown in Figure 2 with the image force lowering included. Figure 3a,b show the obtained Schottky barriers ϕ_B of metal/GaAs and metal/graphene/GaAs junctions as a function of metal work-function ϕ_M . From the I-V measurements, the pinning factor S , defined to be $\partial\phi_B/\partial\phi_M$ [32–34], are obtained to be 0.092 and -0.365 for metal/GaAs and metal/graphene/GaAs junctions, respectively. As mentioned previously, it is quite interesting that the Schottky barrier of metal/graphene/GaAs junction decreases as the metal work-function increases, reflected on the negative value (-0.365) of S . In normal circumstances, the pinning factor ranges between 0 and 1 depending on the pinning strength. In case of IPE measurements, the Schottky barriers for metal/GaAs and metal/graphene/GaAs junctions are extracted to be very similar to each other for all the metals except for Pt. Just as a reminder, the IPE spectrum for Pt/graphene/GaAs couldn't be obtained due to the large junction leakage. The pinning factors in the IPE measurements are found to be 0.012 and 0.008 for metal/GaAs and

metal/graphene/GaAs junctions, respectively, both indicating strong Fermi-level pinning effect.

Based on the I-V and IPE measurements described above, it seems plausible to conclude the following spatial distributions for the interface Fermi-level pinning and associated current flows in metal/GaAs and metal/graphene/GaAs junctions. For metal/GaAs junctions, as shown in Figure 4a,b, the entire region of GaAs surface will have high interface-trap density due to oxidation (native oxide, Figure 4a) or material intermixing with metal atoms (Figure 4b) [12–17]. Hence, the interface Fermi-level pinning effect will appear to be strong throughout the entire region of junction and the junction current will be distributed uniformly (Figure 4e). In case of metal/graphene/GaAs junctions, the prevailing region with regular native oxides will have a large density of interface-trap states (Figure 4c) and the Fermi-level pinning on this region will be strong similarly to the metal/GaAs junction case. Meantime, the small patches with very thin or no native oxide layer will maintain low interface-trap density thanks to the protection of graphene interlayer (Figure 4d) and the observed negative Fermi-level pinning will occur here. Due to the negative pinning, these small patches will have current flows comparable to the surrounding regions for *low* work-function metal electrodes (Figure 4f) forming relatively high interface energy barriers. On the other hand, the current flow through the small patches will be a lot more in comparison with the surrounding regions for *high* work-function metal electrodes (Figure 4g) bearing leaky current paths with low interface energy barriers.

B. Calculated energy band profile across junction

In order to understand the unusual negative Fermi-level pinning in the metal/graphene/GaAs junction, the electron energy band profiles across the junction were obtained by performing finite element electrostatic mod-

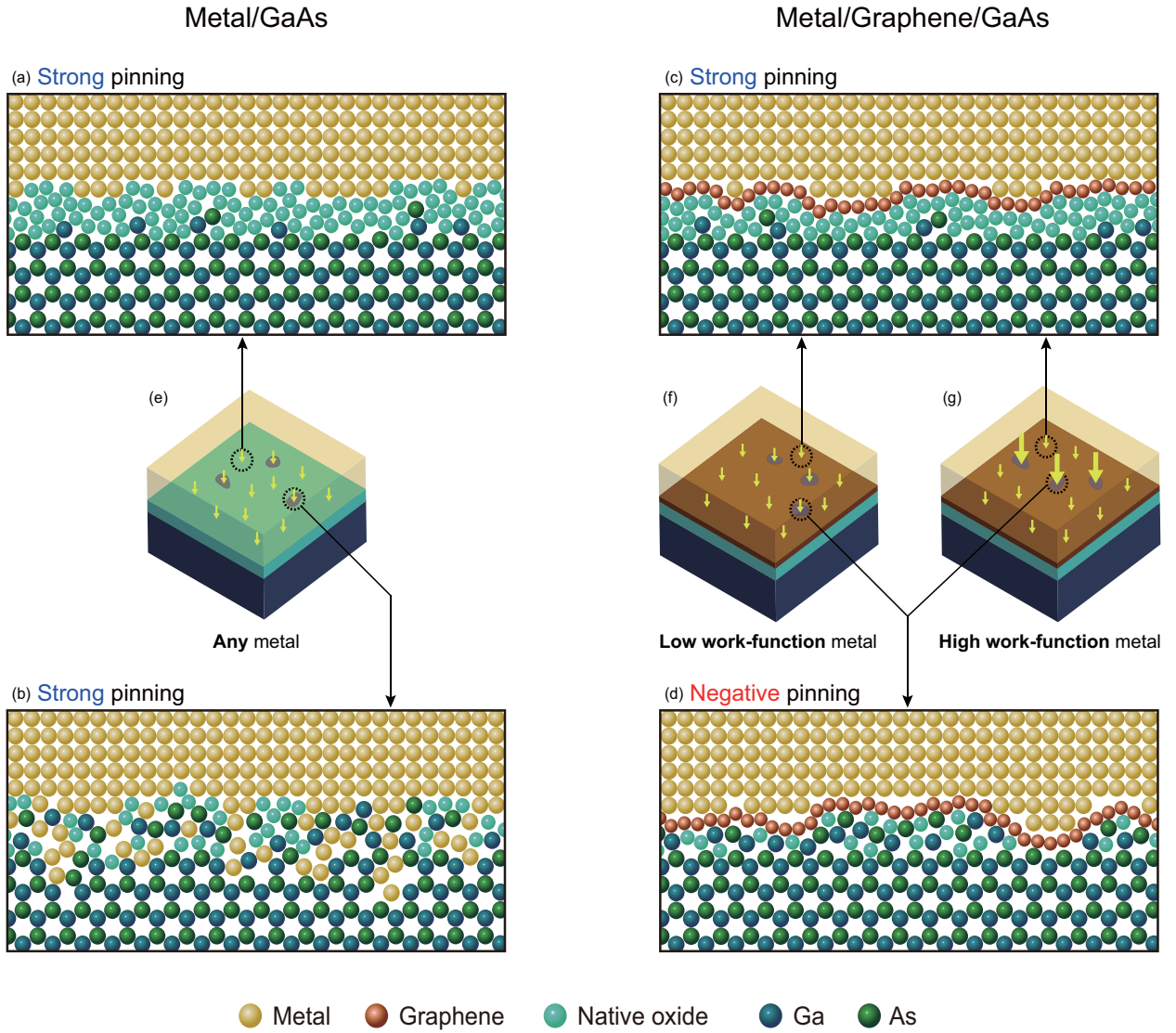


FIG. 4. Atomic arrangement at interface. (a)-(d) Cross-sectional schematics of atomic arrangements at the interfaces of metal/GaAs and metal/graphene/GaAs junctions reflecting the spatial-inhomogeneity of native oxide layer. (e)-(g) Schematics of metal/GaAs and metal/graphene/GaAs junctions with low and high metal work-functions. The black dashed circles in (e)-(g) are linked to the corresponding atomic arrangements at interfaces in (a)-(d). The size of yellow arrows indicates the relative magnitude of junction current.

eling with a commercial software package FlexPDE [35–37] (see Supporting Information for details on the finite element electrostatic modeling). All parameters were implemented with the values measured or reported in the literature [33, 38–41]. The key variable in our modeling is the interaction dipole charge density (Q_D) at metal/graphene contact which was supported by density functional theory (DFT) calculations to exist due to the off-centric distribution of the overlapped electron wavefunctions in the gap between metal and graphene layer [1, 2]. Here, we note that Q_D indicates the charges of interaction dipole layer on the graphene side. First of all, we have calculated the Schottky barrier (ϕ_B) and pinning strength (S) for various interface-trap density

(D_{it}) on GaAs surface by assuming $Q_D = 0$ in order to verify whether or not the observed negative Fermi-level pinning can occur without the interaction dipole layer. If we do not consider the interaction dipole layer, the pinning strength is always calculated to be positive for $10^{12} \text{ eV}^{-1} \cdot \text{cm}^{-2} \leq D_{it} \leq 10^{15} \text{ eV}^{-1} \cdot \text{cm}^{-2}$ which is the typical range for III-V compound semiconductors [38] (see Table S1 in Supporting Information). In addition, if we estimate the Q_D to match with the I-V measured ϕ_B for $D_{it} \geq 10^{13} \text{ eV}^{-1} \cdot \text{cm}^{-2}$, the Q_D increases dramatically to have the physically impossible values (see Table S2 in Supporting Information). This confirms that the negative Fermi-level pinning effect observed in the I-V measurements should occur on the region with low interface-

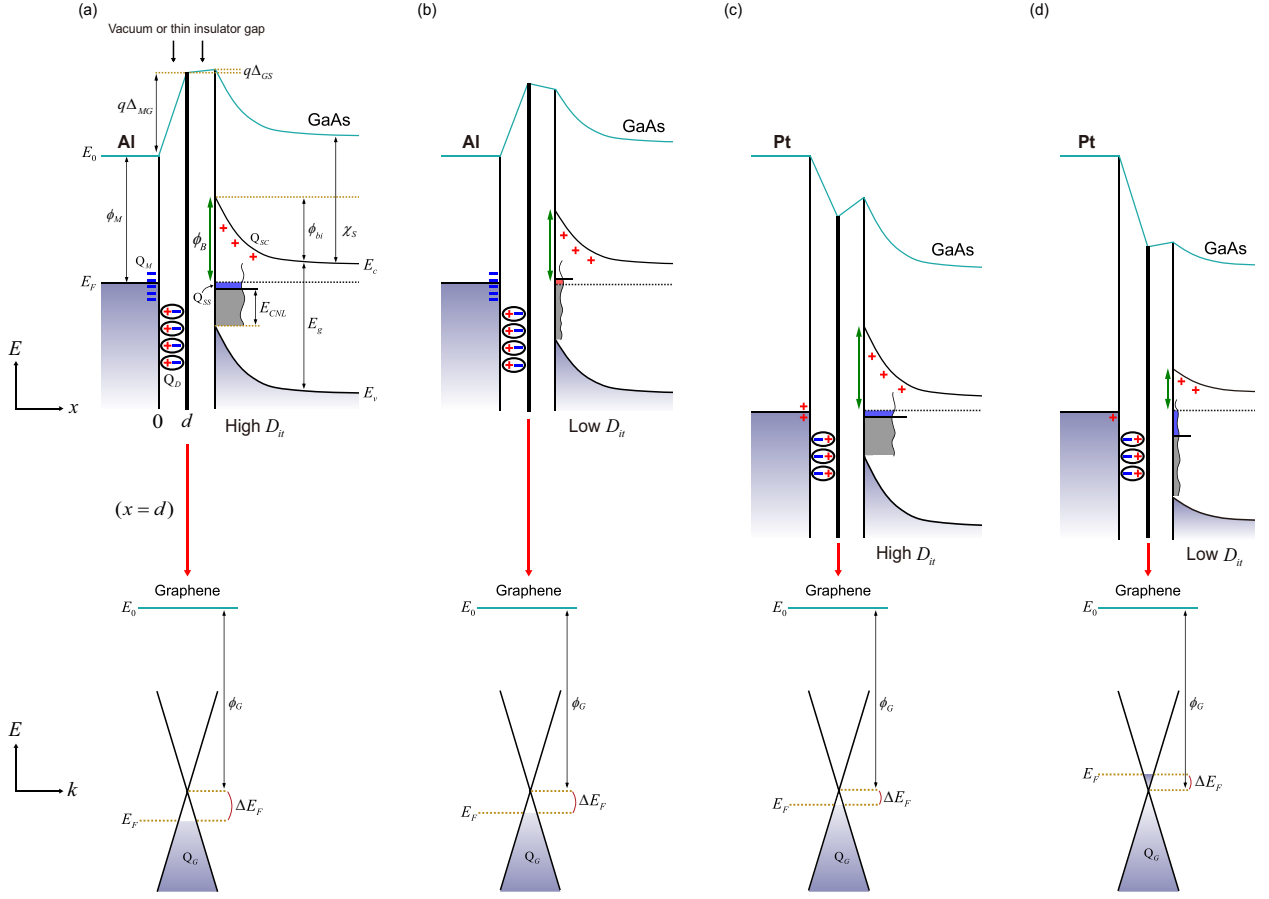


FIG. 5. Energy band alignments. (a)-(d) Energy band alignments of Al/graphene/GaAs and Pt/graphene/GaAs junctions for high (a, c) and low (b, d) interface-trap density (D_{it}) regions. Each of the energy band profiles shown in the upper side is drawn as a function of position in the junction (the metal surface is set to be $x = 0$) and the corresponding linear energy dispersion relation of graphene with the Fermi-level indicated is drawn below each band profile. Δ_{MG} : Potential change across metal/graphene interface, Δ_{GS} : Potential change across graphene/GaAs interface, E_0 : Vacuum level, E_F : Metal Fermi-level, E_c : Conduction band edge, E_v : Valence band edge. ϕ_M : Metal work-function, ϕ_B : Schottky barrier, ϕ_{bi} : Built-in potential, χ_S : Electron affinity of GaAs, E_g : Band gap of GaAs, E_{CNL} : Charge neutrality level of GaAs, Q_M : Free charge density on metal surface, Q_D : Interaction dipole charge density at metal/graphene contact, Q_{SS} : interface-trap charge density on GaAs surface, Q_{SC} : Space charge density in the depletion region of GaAs substrate, ΔE_F : Fermi-level shift of graphene, ϕ_G : Graphene work-function, and Q_G : Doping charge density of graphene.

trap density ($D_{it} \leq 10^{13} \text{ eV}^{-1} \cdot \text{cm}^{-2}$) as concluded from the IPE measurements. Since the interaction dipole layer at metal/graphene contact is expected to be uniformly formed throughout the entire contact, it is reasonable to assume that each metal will have a certain constant Q_D in metal/graphene/GaAs junction regardless of the locally-varying D_{it} on GaAs surface. In the electrostatic modeling, we adopted the Q_D obtained for $D_{it} = 5 \times 10^{12} \text{ eV}^{-1} \text{ cm}^{-2}$ to fit the I-V measured ϕ_B and $D_{it} = 5 \times 10^{14} \text{ eV}^{-1} \text{ cm}^{-2}$ was used for the prevailing region with high interface-trap density. The calculated relevant potentials and charges are listed (see Table S3 in Supporting Information) and the band profiles of Al/graphene/GaAs and Pt/graphene/GaAs junctions are shown in Figure 5 as the representatives of low and high work-function metal electrodes.

C. Electronegativity difference and interaction dipole charge

Figure 6a shows the Schottky barriers extracted from the modeling for four different combinations of Q_D and D_{it} . As seen in the figure, the negative pinning factor for metal/graphene/GaAs junction is obtained only with non-zero Q_D for low D_{it} . In case of Pt/graphene/GaAs junction, it is found that Q_D should be positive to obtain the Schottky barrier measured to be small. This polarity actually coincides with the DFT calculation results mentioned previously [1, 2]. Meanwhile, Q_D for Al/graphene/GaAs junction is found to be negative to match with the measured Schottky barrier. According to the DFT calculations, Q_D for the Al/graphene/GaAs junction will still be positive although its magnitude

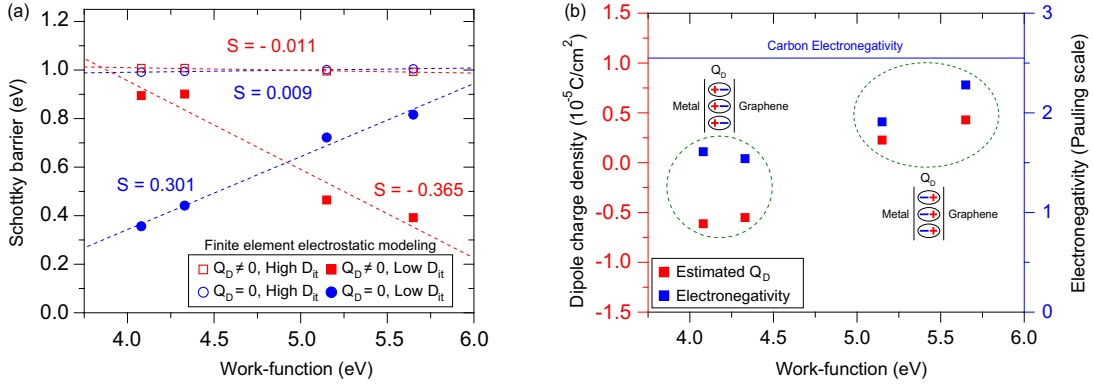


FIG. 6. Calculated pinning strength, correlation of electronegativity and interaction dipole charge. (a) The Schottky barrier of metal/graphene/GaAs junction obtained from the electrostatic modeling as a function of metal work-function for high ($5 \times 10^{14} \text{ eV}^{-1} \text{ cm}^{-2}$) and low ($5 \times 10^{12} \text{ eV}^{-1} \text{ cm}^{-2}$) D_{it} . The modeling is performed for both $Q_D = 0$ and $Q_D \neq 0$. Here, D_{it} is interface-trap density on GaAs surface and Q_D is the interaction dipole charge density at metal/graphene contact. The extracted pinning factor $S = \partial\phi_B/\partial\phi_M$ for each case is also labeled. (b) The Q_D obtained from the electrostatic modeling and the electronegativity of metal atom reported in the previous study [43] as a function of metal work-function. The green dashed circles indicate two distinct groups with opposite polarities of Q_D and the corresponding interaction dipole configurations are also shown.

becomes much smaller than that of Pt/graphene/GaAs junction. However, the positive Q_D will lower the Schottky barrier always, relative to the junction without the graphene interlayer, since the electrostatic potential drops across the gap between metal and graphene layer. Our electrostatic modeling indicates clearly that the Schottky barrier of Al/graphene/GaAs junction is quite low with zero or positive Q_D . Thus it seems inevitable for Q_D to be negative for bearing the experimentally-measured large Schottky barrier.

It is known well that the exchange correlation potential for electrons is attractive in front of a metal surface and the electrons of an atom adsorbed on the metal surface is attracted toward the metal side [42]. Hence, the positive Q_D is quite understandable in terms of this exchange correlation. Then, the question is what induces the negative Q_D of Al/graphene/GaAs junction. One possibility that we can think of is the electronegativity difference between metal and carbon atom. Figure 6b shows the Q_D obtained from the electrostatic modeling and the electronegativity [43] of a metal atom as a function of metal work-function. As shown in the figure, the electronegativities of all the metals used in our work are smaller than that of carbon. This implies that the interacting electrons between metal and graphene will be attracted more toward the graphene side. Especially, the electronegativities of Al and Ti with relatively low work-functions are quite small in comparison with carbon. Accordingly, the driving force shifting the interacting electrons toward the graphene side can be significant, overcoming the tendency of shifting them toward the metal side due to the exchange correlation and leading to the negative Q_D . For Ni and Pt with relatively high work-functions, the difference of electronegativity from carbon becomes smaller.

Therefore, in this case, the interacting electrons are expected to be shifted toward the metal by more prominent exchange correlation so that the positive Q_D is induced. Here, it is noted that the mechanism described above is only a possibility relying on the two known factors of exchange correlation and atomic electronegativity which have been addressed independently. One point consistent between the DFT calculation and our electrostatic modeling is that the tendency of shifting the interacting electrons toward the metal side is reduced significantly for low work-function metals. However, what is apparent from the fundamental physics standpoint, supported from the electrostatic modeling, is that the sign change of Q_D is the essential requirement for the negative Fermi-level pinning observed in our experiments.

IV. CONCLUSIONS

In conclusion, we report the negative Fermi-level pinning effect observed experimentally in metal/graphene/n-GaAs(001) junction. The low interface-trap density regions, protected by the graphene interlayer, are found to have the local Schottky barrier affected directly by the interaction dipole layer at metal/graphene contact. In order to explain the observed negative Fermi-level pinning, it is found that the interacting electrons at the metal/graphene interface should be attracted more toward the graphene side for low work-function metals, bearing the increase of electrostatic potential across the interface. For high work-function metals, they should be attracted more toward the metal side, making the electrostatic potential decrease across the interface accordingly. Based on our

work, it can be claimed that the graphene interlayer can invert the effective work-function of metal between high and low, making it possible to form both Schottky and Ohmic-like contacts with identical (particularly *high* work-function) metal electrodes on a semiconductor substrate possessing low surface-state density.

AUTHOR CONTRIBUTIONS

H.H.Y and K.P. conceived and designed the experiments. H.H.Y., J.K., and K.M. fabricated the devices. H.H.Y. and W.S. performed the measurements. H.H.Y., W.S., S.J., J.K., K.M., G.C., and K.P. analyzed the measured data. W.S. and S.J. performed the electrostatic modeling. H.Y.J. and J.H.L. took TEM images. All authors discussed the results and contributed to writing the manuscript. H.H.Y. and W.S. contributed equally to this work.

ACKNOWLEDGEMENTS

This work was supported by Space Core Technology Development Program (2016M1A3A3A02017648), Basic Science Research Program (2016R1A2B4014762, 2019R1F1A1057767), and Global Ph.D Fellowship Program (2015H1A2A1033714) through the National Research Foundation funded from the Ministry of Science and ICT in Korea. This work has also benefited from the use of the facilities at UNIST Central Research Facilities.

* kibogpark@unist.ac.kr

- [1] Giovannetti, G.; et al. Doping graphene with metal contacts. *Phys. Rev. Lett.* **2008**, *101*, 4.
- [2] Khomyakov, P. A.; et al. First-principles study of the interaction and charge transfer between graphene and metals. *Phys. Rev. B* **2009**, *79*, 12.
- [3] Song, S. M.; Park, J. K.; Sul, O. J.; Cho, B. J. Determination of work Function of graphene under a metal electrode and Its role in contact resistance. *Nano. Lett.* **2012**, *12*, 3887-3892.
- [4] Allain, A.; Kang, J. H.; Banerjee, K.; Kis, A. Electrical contacts to two-dimensional semiconductors. *Nat. Mater.* **2015**, *14*, 1195-1205.
- [5] Xu, Y.; et al. Contacts between two- and three-dimensional materials: ohmic, Schottky, and p-n heterojunctions. *ACS. Nano.* **2016**, *10*, 4895-4919.
- [6] Yoon, H. H.; et al. Strong Fermi-level pinning at metal/n-Si(001) interface ensured by forming an intact Schottky contact with a graphene Insertion layer. *Nano. Lett.* **2017**, *17*, 44-49.
- [7] Byun, K. E.; et al. Graphene for true ohmic contact at metal-semiconductor junctions. *Nano. Lett.* **2013** *13*, 4001-4005.
- [8] Lee, M. H. et al. Two-Dimensional Materials Inserted at the Metal/Semiconductor Interface: Attractive Candidates for Semiconductor Device Contacts. *Nano. Lett.* **2018**, *18*, 4878-4884.
- [9] Baek, S. H. C.; et al. Alleviation of Fermi-level pinning effect at metal/germanium interface by the insertion of graphene layers. *Appl. Phys. Lett.* **2014**, *105*, 4.
- [10] Kim, W.; et al. Tunable graphene-GaSe dual heterojunction device. *Adv. Mater.* **2016**, *28*, 1845-1852.
- [11] Brillson, L. J. *Surfaces and Interfaces of Electronic Materials*; John Wiley & Sons, 2010; Vol. 7.
- [12] Drummond, T. J. Schottky barriers on GaAs: screened pinning at defect levels. *Phys. Rev. B* **1999**, *59*, 8182-8194.
- [13] Altuntas, H.; Altindal, S.; Ozcelik, S.; Shtrikman, H. Electrical characteristics of Au/n-GaAs Schottky barrier diodes with and without SiO₂ insulator layer at room temperature. *Vacuum* **2009**, *83*, 1060-1065.
- [14] Flores, F.; Perez, R.; Rincon, R.; Saizpardo, R. Electron-states at semiconductor interfaces - the intrinsic and extrinsic charge neutrality levels. *Philos. Trans. R. Soc. Lond. Ser. A-Math. Phys. Eng. Sci.* **1993**, *344*, 567-577.
- [15] Spicer, W. E.; Newman, N.; Spindt, C. J.; Lilientalweber, Z.; Weber, E. R. Pinning and Fermi level movement at GaAs-surfaces and interfaces. *J. Vac. Sci. Technol. A-Vac. Surf. Films.* **1990**, *8*, 2084-2089.
- [16] Cheng, C. P.; et al. Atomic nature of the Schottky barrier height formation of the Ag/GaAs(001)-2 x 4 interface: an in-situ synchrotron radiation photoemission study. *Appl. Surf. Sci.* **2017**, *393*, 294-298.
- [17] Suyatin, D. B.; et al. Strong Schottky barrier reduction at Au-catalyst/GaAs-nanowire interfaces by electric dipole formation and Fermi-level unpinning. *Nat. Commun.* **2014**, *5*, 8.
- [18] Tung, R. T. The physics and chemistry of the Schottky barrier height. *Appl. Phys. Rev.* **2014**, *1*, 54.
- [19] Tung, R. T. Electron-transport at metal-semiconductor interfaces - general-theory. *Phys. Rev. B.* **1992**, *45*, 13509-13523.
- [20] Song, J. S.; et al. Wet chemical cleaning process of GaAs substrate for ready-to-use. *J. Cryst. Growth.* **2004**, *264*, 98-103.
- [21] Rideout, V. A review of the theory and technology for ohmic contacts to group III-V compound semiconductors. *Solid-State Electron.* **1975**, *18*, 541-550.
- [22] Song, J. S.; et al. Reduction of Water-Molecule-Induced Current-Voltage Hysteresis in Graphene Field Effect Transistor with Semi-Dry Transfer Using Flexible Supporter. *J. Appl. Phys.* **2019**, *125*, 184302.
- [23] Ferrari, A. C.; et al. Raman spectrum of graphene and graphene layers. *Phys. Rev. Lett.* **2006**, *97*, 4.
- [24] Afanas'ev, V. V. *Internal Photoemission Spectroscopy: Fundamentals and Recent Advances*; Elsevier, 2014.
- [25] Gigli, G.; et al. Direct assessment of tunable Schottky barriers by internal photoemission spectroscopy. *Appl. Phys. Lett.* **1998**, *73*, 259-261.
- [26] Ke, M. L.; Westwood, D. I.; Matthai, C. C.; Richardson, B. E.; Williams, R. H. Hot-electron transport through Au/GaAs and Au/GaAs/AlAs heterojunction interfaces: ballistic-electron-emission-microscopy measurement and Monte Carlo simulation. *Phys. Rev. B* **1996**, *53*, 4845-4849.
- [27] Bardi, J.; Binggeli, N.; Baldereschi, A. Existence of localized interface states in metal/GaAs(100) junctions: Au

- versus Al contacts. *Phys. Rev. B* **2000**, *61*, 5416-5422.
- [28] Norimatsu, W.; Kusunoki, M. Structural features of epitaxial graphene on SiC {0001} surfaces. *J. Phys. D-Appl. Phys.* **2014**, *47*, 16.
- [29] Torkhov, N. A. Formation of a native-oxide structure on the surface of n-GaAs under natural oxidation in air. *Semiconductors* **2003**, *37*, 1177-1184.
- [30] Talin, A. A.; et al. Time-dependent ballistic electron-emission microscopy studies of a Au/(100)GaAs interface with a native-oxide diffusion barrier. *Appl. Phys. Lett.* **1993**, *62*, 2965-2966.
- [31] Cheung, S. K.; Cheung, N. W. Extraction of Schottky diode parameters from forward current-voltage characteristics *Appl. Phys. Lett.* **1986**, *49*, 85-87.
- [32] Dimoulas, A.; Tsipas, P.; Sotiropoulos, A.; Evangelou, E. K. Fermi-level pinning and charge neutrality level in germanium. *Appl. Phys. Lett.* **2006**, *89*, 3.
- [33] Sze, S. M.; Ng, K. K. *Physics of Semiconductor Devices*; John Wiley & Sons, 2006.
- [34] Cowley, A. M.; Sze, S. M. Surface states and barrier height of metal-semiconductor systems. *J. Appl. Phys.* **1965**, *36*, 3212-&.
- [35] PDE Solutions, Inc., Spokane Valley, WA, U.S.A., <http://www.pdesolutions.com>
- [36] Choi, G.; et al. Schottky barrier modulation of metal/4H-SiC junction with thin interface spacer driven by surface polarization charge on 4H-SiC substrate. *Appl. Phys. Lett.* **2015**, *107*, 5.
- [37] Park, K. B.; et al. Effect of inclined quantum wells on macroscopic capacitance-voltage response of Schottky contacts: Cubic inclusions in hexagonal SiC. *Appl. Phys. Lett.* **2005**, *86*, 3.
- [38] Brammertz, G.; et al. Capacitance-voltage characterization of GaAs-oxide interfaces. *J. Electrochem. Soc.* **2008**, *155*, H945.
- [39] Haynes, W. M. *CRC handbook of chemistry and physics*; CRC press, 2014.
- [40] Tipler, P. A.; Llewellyn, R. A. *Modern physics*; Freeman, 2008.
- [41] Michaelson, H. B. The work function of the elements and its periodicity. *J. Appl. Phys.* **1977**, *48*, 4729.
- [42] Da Silva, J. L. F.; Stampfl, C.; Scheffler, M. Adsorption of Xe Atoms on Metal Surfaces: New Insights from First-Principles Calculations. *Phys. Rev. Lett.* **2003**, *90*, 066104.
- [43] Pearson, R. G. Absolute electronegativity and hardness - application to inorganic-chemistry. *Inorg. Chem.* **1988**, *27*, 734-740.

Supporting Information:

Negative Fermi-level Pinning Effect of Metal/n-GaAs(001) Junction with Graphene Interlayer

Hoon Hahn Yoon,[†] Wonho Song,[†] Sungchul Jung,[†] Junhyung Kim,[‡] Kyuhyung Mo,[†] Gahyun Choi,[†] Hu Young Jeong,[¶] Jong Hoon Lee,[¶] and Kibog Park^{*,†,‡}

[†]*Department of Physics, Ulsan National Institute of Science and Technology (UNIST),
Ulsan 44919, Republic of Korea*

[‡]*School of Electrical and Computer Engineering, Ulsan National Institute of Science and
Technology (UNIST), Ulsan 44919, Republic of Korea*

[¶]*UNIST Central Research Facilities (UCRF), Ulsan National Institute of Science and
Technology (UNIST), Ulsan 44919, Republic of Korea*

E-mail: kibogpark@unist.ac.kr

Phone: +82 (0)52 2172111. Fax: +82 (0)52 2172130

Direct Optical Excitation from Localized Interface States

The IPE yield spectra for metal/GaAs and metal/graphene/ GaAs junctions are shown in Figure 2.^{1,2} As pointed out in the manuscript, the IPE signals will be mainly from the prevailing regions of GaAs surface with high interface-trap density. Two IPE thresholds ϕ_{th} are clearly observed for the conduction band minima (Γ and L valleys) in GaAs.³ The first threshold represents the commonly accepted Schottky barrier of metal/GaAs junction, which reflects the electron transmission from metal into the Γ valley in GaAs. The additional transmission into the L valley in GaAs corresponds to the second threshold. The gap between first and second thresholds is about 0.29 eV, which is in excellent agreement with the known energy separation between Γ and L valleys. However, the observation of additional transmission into the X valley in GaAs is disturbed by the humps of IPE yield around 1.33 eV, which are considered to be caused by the direct optical excitation from the localized interface states below the charge neutrality level to the Γ or L valleys. These localized interface states responsible for the strong Fermi-level pinning at metal/GaAs contact are filled with electrons since they are below the charge neutrality level.⁴ In order to characterize further how the localized interface states contribute to the IPE yield, we measured the IPE yield spectra under applied reverse bias varying from 0.001 V to 5.00 V, as shown in Figure S1. The humps around 1.33 eV are found for all metal electrodes although there is a certain degree of metal dependence in the relative strength of hump. It is readily noticeable that the hump become more pronounced with the applied bias increasing. This indicates that more and more electrons excited from the localized interface states can escape and transmit into the conduction band minima of GaAs with the aid of the electric field in the depletion region due to the applied bias.

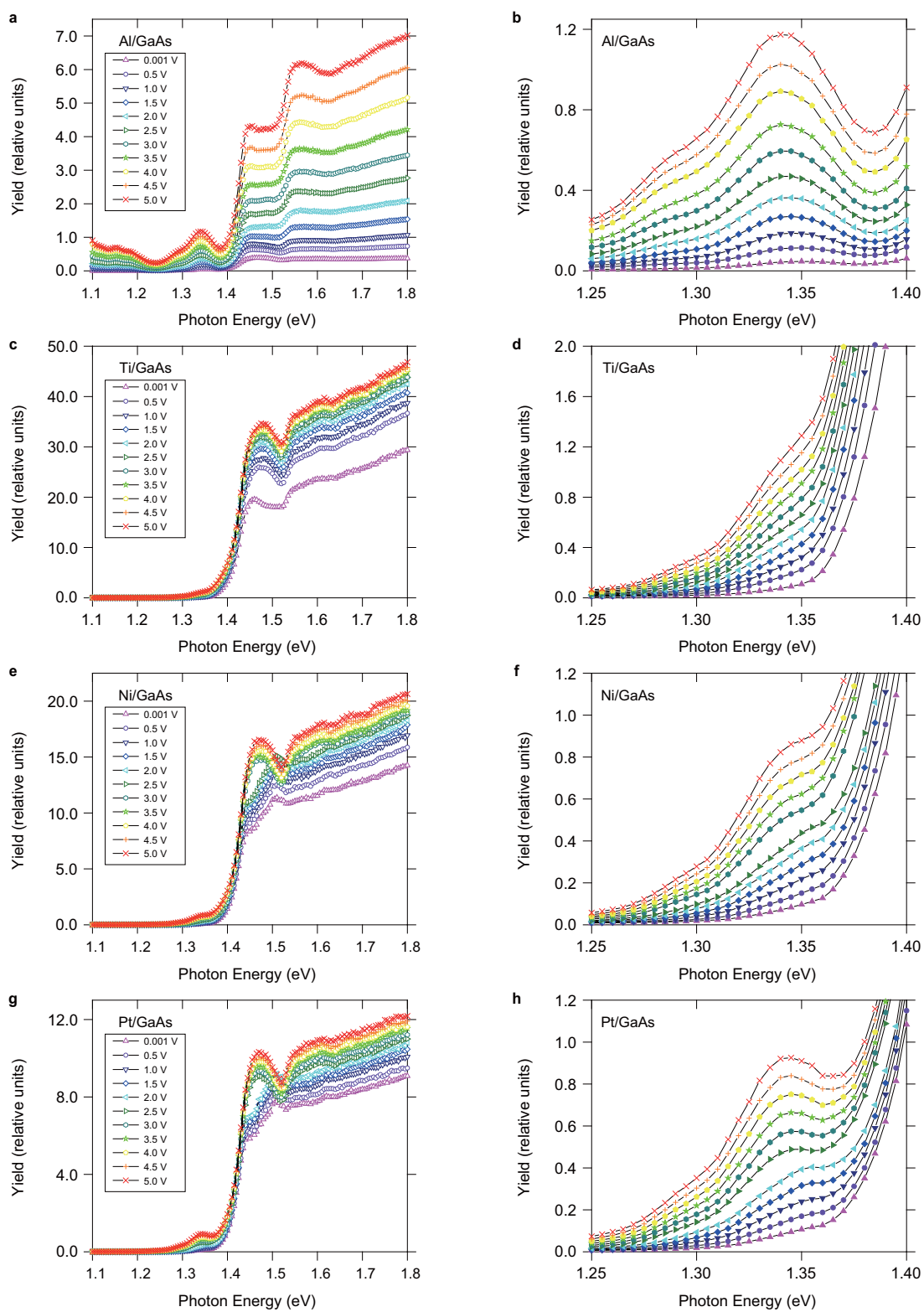


Figure S1: IPE quantum yield as a function of photon energy measured on the metal/GaAs junctions with Al (a), Ti (c), Ni (e), and Pt (g) electrodes under applied reverse bias varying from 0.001 to 5 V. The magnified views of the curves around 1.33 eV are shown in (b), (d), (f), and (h).

Finite Element Electrostatic Modeling

Finite element electrostatic modeling has been performed to find the electron energy band alignment of metal/graphene/GaAs junction for high and low interface-trap density regions with a commercial software package FlexPDE.⁵⁻⁷

The electrostatic potential drop U from the vacuum level on the metal electrode side was calculated by solving the Poisson's equation $\nabla^2 U(x) = -\frac{\rho(x)}{\varepsilon_0 \varepsilon_r}$, where $\rho(x)$ is the net charge density, ε_0 is the permittivity of vacuum, and ε_r is the dielectric constant. The net charge density is assumed to be zero in the vacuum gaps (metal/graphene or graphene/GaAs contact) and is given as $\rho(x) = q[N_D - n(x)]$ in the GaAs substrate, where q is the electronic charge, $N_D = 5 \times 10^{16} \text{ cm}^{-3}$ is the doping concentration of n-GaAs, $n = N_C \exp(-\frac{E_C - E_F}{k_B T})$ is the concentration of free electron in GaAs, N_C is the effective density of states in the conduction band of GaAs, $E_C(x) = \phi_M - \chi_S - qU(x)$ is the conduction band edge of GaAs, E_F is the Fermi-level, $k_B T$ is the thermal energy, ϕ_M is the metal work-function, and χ_S is the electron affinity of GaAs.

We define the metal surface to be at $x = 0$, the vacuum gap between metal surface and graphene layer in $0 < x < d$, the graphene layer at $x = d$, the vacuum gap between graphene layer and GaAs substrate in $d < x < 2d$, and the GaAs substrate in $2d < x < X$ as shown in Figure S2. It is considered that the thin charge sheets Q_M , Q_G , and Q_{SS} are located at $x = 0$, $x = d$, and $x = 2d$,⁸⁻¹¹ where Q_M is the surface free charge density on the metal surface, $Q_G = \frac{q \Delta E_F |\Delta E_F|}{\pi \hbar^2 v_F^2}$ is the doping charge density of graphene, $Q_{SS} = -q D_{it} (E_g - E_{CNL} - \phi_B)$ is the interface-trap charge density on GaAs surface, $\Delta E_F = \phi_M - \phi_G - qU(d)$ is the Fermi-level shift from Dirac point of graphene, \hbar is the reduced Planck constant, v_F is the Fermi velocity of graphene, ϕ_G is the graphene work-function, D_{it} is the interface-trap density on GaAs surface, E_g is the band gap of GaAs, E_{CNL} is the charge neutrality level of GaAs determined from the I-V and IPE measurements in this work, and $\phi_B = \phi_M - \chi_S - qU(2d)$ is the Schottky barrier of metal/graphene/GaAs junction. We assume that two opposite sign of interaction dipole charges are located at $x = 0$ and $x = d$ and Q_D represents the

interaction dipole charge density on the graphene side.

The boundary conditions are assigned as $U(0) = 0$, $U(2d + X) = \phi_M - \chi_S - k_B T \ln(\frac{N_C}{N_D})$, $\lim_{\epsilon \rightarrow 0} \int_{d-\epsilon}^{d+\epsilon} \rho(x) dx = Q_G + Q_D$, and $\lim_{\epsilon \rightarrow 0} \int_{2d-\epsilon}^{2d+\epsilon} \rho(x) dx = Q_{SS}$. From the modeling, the Schottky barrier ϕ_B , the voltage drop across metal/graphene interface $\Delta_{MG} = \frac{(Q_M - Q_D)}{C}$, the voltage drop across graphene/GaAs interface $\Delta_{GS} = -\frac{(Q_{SS} + Q_{SC})}{C}$, and the Fermi-level shift ΔE_F of graphene can be obtained,⁸⁻¹¹ where $C = \frac{\epsilon_0}{d}$ is the capacitance of vacuum gap per unit area, $Q_{SC} = \sqrt{2\epsilon_0\epsilon_r N_D(\phi_{bi} - k_B T)}$ is the space charge density in GaAs, and $\phi_{bi} = \phi_B - k_B T \ln(\frac{N_C}{N_D})$ is the built-in potential energy. The sign of ΔE_F is determined by the charge carrier type of graphene, that is, $\Delta E_F > 0$ for p-type graphene and $\Delta E_F < 0$ for n-type graphene. Note that the depletion region completely ends way before the edge of calculation domain ($x = 2d + X$) with the thickness of 500 nm for the GaAs substrate so that no difference in calculation results is made from using the actual thickness of GaAs substrate (0.5 mm).

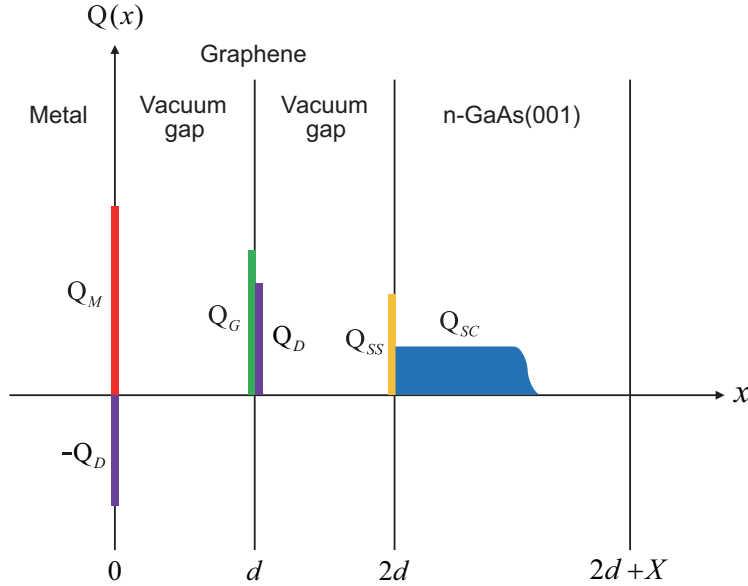


Figure S2: Charge distribution across metal/graphene/GaAs junction, where Q_M is the surface free charge density on metal, Q_D is the interaction dipole charge density at metal/graphene contact, Q_G is the doping charge density of graphene, Q_{SS} is the interface-trap charge density on GaAs surface, Q_{SC} is the space charge density in the depletion region of GaAs substrate, d is the thickness of vacuum gap, and X is the thickness of GaAs substrate.

Table S1: The calculated ϕ_B and pinning strength S by assuming $Q_D = 0$ and varying D_{it} for the metal/graphene/GaAs junctions with Al, Ti, Ni, and Pt electrodes.

D_{it} ($\text{eV}^{-1}\cdot\text{cm}^{-2}$)		0	1×10^{12}	5×10^{12}	1×10^{13}	5×10^{13}	1×10^{14}	5×10^{14}	1×10^{15}
Calculated ϕ_B (eV) (assuming $Q_D = 0$)	Al	0.187	0.229	0.356	0.459	0.704	0.766	0.826	0.834
	Ti	0.283	0.322	0.442	0.535	0.738	0.784	0.829	0.836
	Ni	0.681	0.691	0.722	0.746	0.805	0.821	0.937	0.840
	Pt	0.808	0.810	0.816	0.821	0.834	0.838	0.841	0.842
S		0.412	0.384	0.301	0.234	0.082	0.045	0.010	0.005

Table S2: The estimated Q_D to match with the I-V measured ϕ_B by varying D_{it} for the metal/graphene/GaAs junctions with Al, Ti, Ni, and Pt electrodes.

D_{it} ($\text{eV}^{-1}\cdot\text{cm}^{-2}$)		0	1×10^{12}	5×10^{12}	1×10^{13}	5×10^{13}	1×10^{14}	5×10^{14}	1×10^{15}
Estimated Q_D (10^{-6} C $\cdot\text{cm}^{-2}$) (to fit with the I-V measured ϕ_B)	Al	-5.87	-5.92	-6.13	-6.39	-8.62	-11.84	-54.48	-149.98
	Ti	-5.23	-5.29	-5.52	-5.81	-8.35	-12.05	-62.69	-178.49
	Ni	1.60	1.74	2.27	3.09	18.61	60.31	1286.07	5048.71
	Pt	3.35	3.51	4.29	5.58	28.57	89.08	1843.13	7210.81

Table S3: Calculated relevant potentials (ϕ_B , ΔE_F , Δ_{MG} , Δ_{GS}) and charges (Q_M , Q_G , Q_{SS} , Q_{SC}) for metal/graphene/GaAs junctions with Al, Ti, Ni, and Pt electrodes. The calculation has been performed for high $D_{it} = 5 \times 10^{14}$ $\text{eV}^{-1} \text{cm}^{-2}$ and low $D_{it} = 5 \times 10^{12}$ $\text{eV}^{-1} \text{cm}^{-2}$ with fixed Q_D obtained for $D_{it} = 5 \times 10^{12}$ $\text{eV}^{-1} \text{cm}^{-2}$ in Table S2.

Metal	Al		Ti		Ni		Pt	
ϕ_M (eV) ¹²⁻¹⁴	4.08		4.33		5.15		5.65	
Q_D (10^{-6} C $\cdot\text{cm}^{-2}$)	-6.13		-5.52		2.27		4.29	
D_{it} ($\text{eV}^{-1}\cdot\text{cm}^{-2}$)	5×10^{12}	5×10^{14}	5×10^{12}	5×10^{14}	5×10^{12}	5×10^{14}	5×10^{12}	5×10^{14}
E_{CNL} (eV)	0.582	0.413	0.582	0.413	0.582	0.413	0.582	0.413
ϕ_B (eV)	0.895	1.008	0.901	1.008	0.465	0.995	0.392	0.993
ΔE_F (eV)	0.521	0.539	0.529	0.546	-0.039	0.167	-0.135	0.106
Δ_{MG} (V)	0.941	0.959	0.699	0.716	-0.689	-0.483	-1.285	-1.044
Δ_{GS} (V)	-0.056	0.039	-0.058	0.032	0.074	0.398	0.097	0.456
Q_M (10^{-6} C $\cdot\text{cm}^{-2}$)	-3.364	-3.306	-3.467	-3.412	0.234	0.848	0.498	1.215
Q_G (10^{-6} C $\cdot\text{cm}^{-2}$)	3.197	3.424	3.295	3.511	-0.018	0.328	-0.216	0.133
Q_{SS} (10^{-6} C $\cdot\text{cm}^{-2}$)	0.042	-0.251	0.047	-0.231	-0.302	-1.308	-0.361	-1.480
Q_{SC} (10^{-6} C $\cdot\text{cm}^{-2}$)	0.125	0.133	0.125	0.133	0.087	0.132	0.079	0.132

Raman Spectrum Measurements

The confocal Raman spectroscopy with the laser wavelength of 532 nm has been carried out for the transferred graphene on GaAs substrate. The measured spectra are shown in Figure S3. The intensity ratio between the G peak ($\sim 1580\text{ cm}^{-1}$) and the 2D peak ($\sim 2700\text{ cm}^{-1}$) indicates that the transferred graphene is a monolayer.¹⁵

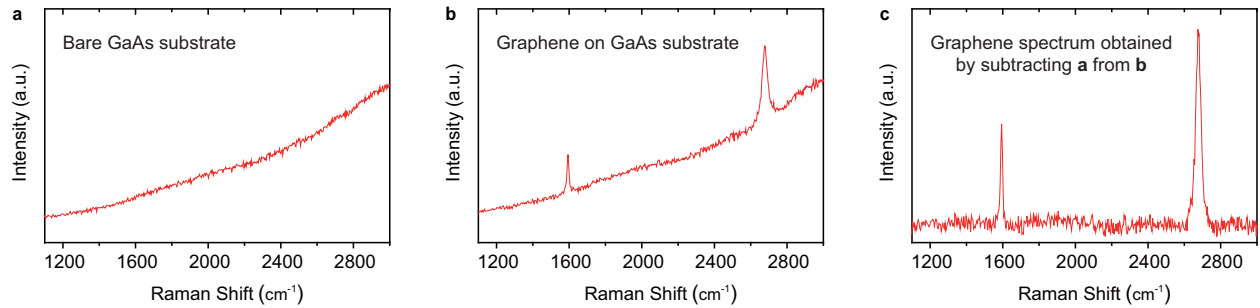


Figure S3: Raman spectrum measurements of the graphene used in this work. The Raman spectra of bare GaAs substrate (a), graphene on GaAs substrate (b), and graphene with the GaAs background signal subtracted (c).

Transmission Electron Microscope Images

After all the electrical measurements were completed, transmission electron microscope images were obtained. The bright-field TEM (BFTEM) and high-resolution TEM (HRTEM) images of Pt/GaAs and Pt/graphene/GaAs junctions are shown in Figure S4. The graphene layer inserted at Pt/GaAs interface is seen clearly.¹⁶ It is confirmed with HRTEM images taken on the several different sites in the Pt/GaAs (Figure S4b,c) and Pt/graphene/GaAs (Figure S4e,f) junctions that the thickness of native oxide layer is spatially inhomogeneous. In addition, the area of GaAs surface occupied with very thin or no native oxide layer is found to be quite small, indicated by red circles. The thickness of oxide layer on GaAs surface is estimated about ~ 2.82 nm for Pt/GaAs junction and ~ 2.27 nm for Pt/graphene/GaAs junction.¹⁷ It is likely to have slightly thicker oxide layer for Pt/GaAs junction compared to that for Pt/graphene/GaAs junction on the same GaAs substrate because the oxide layer on the graphene-covered area was passivated while the oxide layer on the graphene-uncovered area was exposed to the air before the metal electrode deposition. Since the native GaAs oxide is found to have very small band gap,¹⁸ the charge carrier transport across metal/GaAs junction depends significantly on whether the graphene layer is inserted at the interface or not rather than the small difference in the thickness of GaAs oxide layer.

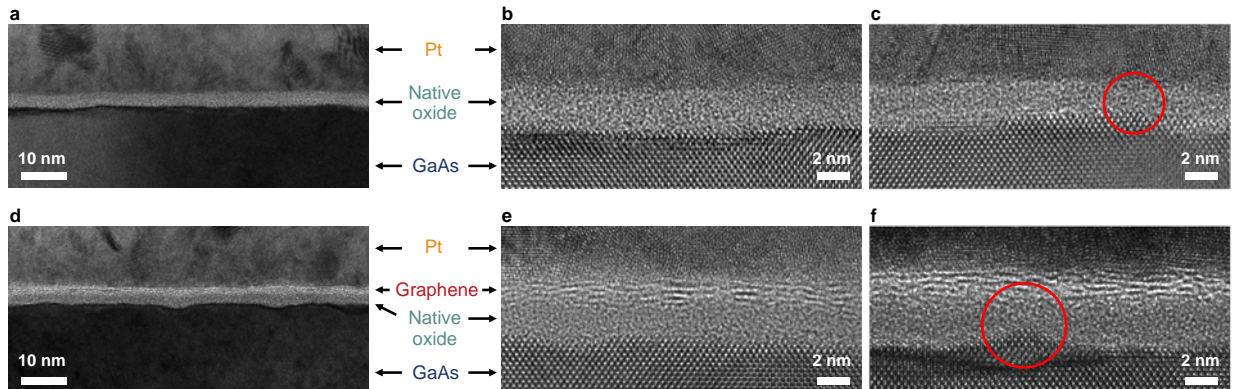


Figure S4: BFTEM (a) and HRTEM (b, c) images of Pt/GaAs junction. BFTEM (d) and HRTEM (e, f) images of Pt/graphene/GaAs junction. The red circles represent the small-size regions with very thin native oxide layer.

References

- (1) Afanas'ev, V. V. *Internal Photoemission Spectroscopy: Fundamentals and Recent Advances*; Elsevier, 2014.
- (2) Gigli, G.; et al. Direct assessment of tunable Schottky barriers by internal photoemission spectroscopy. *Appl. Phys. Lett.* **1998**, *73*, 259-261.
- (3) Ke, M. L.; Westwood, D. I.; Matthai, C. C.; Richardson, B. E.; Williams, R. H. Hot-electron transport through Au/GaAs and Au/GaAs/AlAs heterojunction interfaces: ballistic-electron-emission-microscopy measurement and Monte Carlo simulation. *Phys. Rev. B* **1996**, *53*, 4845-4849.
- (4) Bardi, J.; Binggeli, N.; Baldereschi, A. Existence of localized interface states in metal/GaAs(100) junctions: Au versus Al contacts. *Phys. Rev. B* **2000**, *61*, 5416-5422.
- (5) PDE Solutions, Inc., Spokane Valley, WA, U.S.A., <http://www.pdesolutions.com>
- (6) Choi, G.; et al. Schottky barrier modulation of metal/4H-SiC junction with thin interface spacer driven by surface polarization charge on 4H-SiC substrate. *Appl. Phys. Lett.* **2015**, *107*, 5.
- (7) Park, K. B.; et al. Effect of inclined quantum wells on macroscopic capacitance-voltage response of Schottky contacts: Cubic inclusions in hexagonal SiC. *Appl. Phys. Lett.* **2005**, *86*, 3.
- (8) Kim, W.; et al. Tunable graphene-GaSe dual heterojunction device. *Adv. Mater.* **2016**, *28*, 1845-1852.
- (9) Tung, R. T. The physics and chemistry of the Schottky barrier height. *Appl. Phys. Rev.* **2014**, *1*, 54.
- (10) Sze, S. M.; Ng, K. K. *Physics of Semiconductor Devices*; John Wiley & Sons, 2006.

- (11) Cowley, A. M.; Sze, S. M. Surface states and barrier height of metal-semiconductor systems. *J. Appl. Phys.* **1965**, *36*, 3212-&.
- (12) Haynes, W. M. *CRC handbook of chemistry and physics*; CRC press, 2014.
- (13) Tipler, P. A.; Llewellyn, R. A. *Modern physics*; Freeman, 2008.
- (14) Michaelson, H. B. The work function of the elements and its periodicity. *J. Appl. Phys.* **1977**, *48*, 4729.
- (15) Ferrari, A. C.; et al. Raman spectrum of graphene and graphene layers. *Phys. Rev. Lett.* **2006**, *97*, 4.
- (16) Norimatsu, W.; Kusunoki, M. Structural features of epitaxial graphene on SiC {0001} surfaces. *J. Phys. D-Appl. Phys.* **2014**, *47*, 16.
- (17) Torkhov, N. A. Formation of a native-oxide structure on the surface of n-GaAs under natural oxidation in air. *Semiconductors* **2003**, *37*, 1177-1184.
- (18) Talin, A. A.; et al. Time-dependent ballistic electron-emission microscopy studies of a Au/(100)GaAs interface with a native-oxide diffusion barrier. *Appl. Phys. Lett.* **1993**, *62*, 2965-2966.